Active control analysis of mining vehicle cabin noise using finite element modelling

D.A. Stanef, C.H. Hansen*, R.C. Morgans

Department of Mechanical Engineering, Active Noise and Vibration Control Group, The University of Adelaide, Adelaide, South Australia 5005, Australia

Received 26 February 2003; accepted 29 August 2003

Abstract

Numerical simulation has been used to predict the reduction of acoustic potential energy in a mobile mining vehicle cabin as a result of active noise control (ANC). Resonance frequencies and mode shapes of both the structural and cavity modes were calculated using a finite element (FE) model. Modal coupling analysis was used to determine the coupled response of the model to an interior acoustic source, and the results were compared to measurements taken inside the cabin. Correlation between the FE model and physical measurements was improved to the extent that the model could be used to predict the effect of ANC in the cabin for different configurations of control sources and error sensors. As expected from previous work, it was found that the acoustic potential energy inside the cabin could be significantly reduced if a control source is placed in close proximity to the primary volume velocity source. However, increasing the number of sensors and/or increasing the number of control sources located remotely from the primary source had little impact on the achievable reduction in the overall acoustic potential energy in the cabin. This supported results obtained in off-line experiments using control source to error sensor transfer function measurements and quadratic optimization theory, where it was found that good reduction at the error sensors was possible inside the mining vehicle cabin but that global control was not feasible using sources remotely located from the primary source.
© 2003 Elsevier Ltd. All rights reserved.

1. Introduction

Low-frequency noise in the cabins of heavy machinery such as diesel-driven mining vehicles result in drivers experiencing fatigue and high levels of distraction. Here, the effectiveness of applying an active noise control (ANC) system to a Caterpillar mining vehicle cabin is investigated using finite element (FE) modelling.

---

*Corresponding author. Fax: +61-8-8303-4367.
E-mail address: colin.hansen@adelaide.edu.au (C.H. Hansen).

Previous work on applying ANC to enclosures has included analytical, numerical and experimental investigations. In general, results from these studies have indicated that ANC will work in enclosed spaces, provided that the conditions discussed in the following paragraphs are met.

Nelson et al. [1] investigated theoretically the feasibility of global control in an arbitrary enclosure excited at a single frequency under steady state conditions. They concluded that the reduction of acoustic potential energy (PE) in an environment of high modal density is only possible if the control source is located within half a wavelength of the primary source. Bullmore et al. [2] showed that in an acoustical environment of low modal density, global attenuation of sound with a secondary source located further than half a wavelength from the primary source is achievable provided that the secondary source is placed at an antinode of the primary field. Placing sensors in enclosure corners and minimizing the responses there has the greatest effect on reducing acoustic PE in an enclosure when more than one mode dominates. However, for these cases to work, the primary excitation must be at an acoustic resonance.

Elliott et al. [3] attempted an experimental verification of the previous two studies using a simple rectangular enclosure. As predicted by the computer simulation of Bullmore et al. [2], good reductions were achieved only when the enclosure was excited on resonance. Very good correlations between the predicted and measured impedance transfer functions were observed; however, correlations between predicted and observed noise reductions were not accurate. The spatial distributions of the predicted and measured controlled sound fields in the enclosure of interest were similar, but the amplitude of each was not. The average amplitudes of the two fields were manually set equal only to aid comparison. A prediction of the achievable acoustic PE reduction over a narrow frequency range showed that in most cases the acoustic PE would be reduced, but there was a chance of increasing the energy at some frequencies.

Application of ANC to a more complex enclosure was reported by Bullmore et al. [4]. In this paper, a BAe 748 twin turbo-prop aircraft fuselage was modelled theoretically as a thin cylindrical shell and a cylindrical room (with floor). The damping of the aircraft cabin in this case was estimated by matching predicted and experimental results, and found to be approximately 30% across all modes. It was not suggested that the damping for the fuselage was actually as high as 0.3, but that this was the parameter value that must be used in order to obtain reasonable agreement between experimental and theoretical results.

The simulation results by Bullmore et al. [4] showed that for a control system comprised of 32 error sensors and 16 control sources, the achievable average sum of squared pressure reductions over a plane representative of the height of seated passengers was 14 dB for the first propeller blade passage frequency (BPF) of 88 Hz, and 4 dB for the second harmonic.

Elliott et al. [5,6] validated the study by Bullmore et al. [4], achieving broad agreement with the theoretical predictions. Alternative configurations of control sources were tested, with improved control at the second and third harmonics obtained by concentrating the majority of the loudspeakers in the plane of the propellers. The reduction in the tone at the fundamental frequency was a maximum when a fully distributed control source arrangement throughout the cabin was used. When all three harmonics were controlled simultaneously, a less than optimal reduction was recorded at some microphones and an increase in sound level recorded at others.

Also of interest in the paper by Elliott et al. [6] were the results from testing a two-microphone, two-control source ANC system on a passenger seat. A grid was set up that enabled the sound

pressure around the microphones to be measured. As would be expected, reduction down to the noise floor was achieved at the two microphones. Reasonable reductions were also recorded around the controlled microphones up to about 70 mm away. This corresponded to results presented by Elliott et al. [7], where it was shown that, on average, the result of driving the pressure to zero at an error sensor will be a spherical zone of quiet with a diameter about one tenth of the wavelength of the excitation frequency. The sound level within this zone is expected to be at least 10 dB less than the primary level at that location.

Dorling et al. [8] also performed experimental work in the BAe 748 twin turbo-prop aircraft. They predicted and verified the control of the 88 Hz fundamental excitation frequency in the cabin using a 72-microphone, 24-control source ANC system. Reduction of sound pressure at over 50 points in the cabin was measured and compared to reductions predicted using quadratic optimization theory. Reasonable agreement between predicted and experimental data was achieved.

Johansson et al. [9] experimentally investigated the performance of a control system that used two reference signals to attenuate the noise of two propellers entering an aircraft fuselage. In one case two primary sources generated the same frequency and in another the primary noise field comprised of two frequencies separated by 0.5 Hz such that beating occurred. Attenuation of the order of 3–5 dB was achieved at the BPF in the presence of beating, and 18 dB in its absence.

In Thomas et al. [10] a cylindrical shell model of an aircraft fuselage was used to investigate the effectiveness of using structural control sources to attenuate the noise level inside the cabin. The radial component of the kinetic energy in the structure was minimised for control and produced predictions of poor global attenuation inside the cavity. Consequently, Thomas et al. [10] attempted using structural forces to minimise the acoustic PE of the cavity instead. The results from this approach were much more encouraging. Thomas et al. [11] showed that good global reductions of acoustic PE are possible at the two harmonics of interest using relatively few structural sources. In fact, it seemed that better reduction of acoustic PE was achieved using structural force inputs than acoustic sources.

Snyder and Hansen [12] presented a theoretical design methodology for an ANC system in enclosed spaces. The importance of optimising both the physical and electronic parts of the control system was discussed. In Snyder and Hansen [13] it was shown that the mechanism by which the acoustic PE is reduced in an enclosure with acoustic control sources is by source unloading, and that in optimal conditions, the sources should never cause an increase in the acoustic PE.

Zander [14] investigated the effect of control source and error sensor configurations for a simplified light aircraft fuselage. He found that the level of acoustic PE reduction in the aircraft structure was much more a function of the locations of the control sources relative to the primary source, and that as the number of control sources increased, so too did the level of reduction. Also, a higher reduction in acoustic PE was achieved when the primary excitation of the structure was at an acoustic resonance.

In addition to the theoretical methods mentioned above, FE modelling has emerged as a tool that can be used for analyzing an enclosure targeted for ANC. Alvelid [15] investigated how a FE model could be used for simulating the performance of an ANC system on an aircraft structure. He used the model to calculate the reduction possible by minimizing the sum of the quadratic pressures over the cabin using an optimization algorithm. However, no detail was given as to how the model was verified.

Carletti et al. [16] developed a simplistic FE model of an earth-moving cabin and used it to predict the time averaged acoustic PE reduction possible at three frequencies related to engine and cooling system noise. They verified their model by comparing the magnitude of sound level measurements taken in the cab with levels predicted by the model, and achieved good agreement at two out of the three frequencies.

Dai and Fuller [17] showed the importance of control source locations in an ANC system placed in an aircraft fuselage. Optimal positions were calculated to reduce the total acoustic PE in the interior cavity at a single frequency. These locations were entered into a FE model and sound pressure level results were obtained with and without control. Results were then obtained with control sources located in random positions and compared to those obtained with the optimal source locations. Results showed that the optimal locations achieved greater global and local control than locations selected randomly.

Applying modal coupling theory to a FE model was reported by Cazzolato [18], and Cazzolato and Hansen [19]; for a curved panel with simple rectangular backing cavity. By applying modal coupling theory to calculate the coupled structural-cavity response, they achieved good correlation between simulated and measured data for the active control of sound transmission into the enclosure over a range of frequencies.

Cases where more complex structures have been modelled over a range of frequencies have also been reported. Unruh and Dobosz [20] modelled an aircraft fuselage with FE methods, and experimentally verified their model over a frequency range of 100–500 Hz. Using an external shaker as the primary source, they measured the interior noise levels in the fuselage and achieved at worst a 10 dB error between their model and experimental data. Like Bullmore et al. [4], they believed the use of average acoustic modal damping for interior noise prediction worked well. Sung and Nefske [21] investigated the characteristics of a GM van with the aid of FE tools to determine which panels contributed most to noise inside the vehicle. Incorporating modal coupling, their model achieved broad agreement with experimental results over a 20–100 Hz frequency range, although at some frequencies there were discrepancies of more than 20 dB. The loss in accuracy was attributed to increasing modal density at higher frequencies.

Following the literature review, it appears that little work has been done on analyzing complex enclosures with high damping and high modal density with the aid of FE modelling. Attempts to analyze the control of sound over a broad frequency range are also limited. Bullmore et al. [4] targeted the constant operating frequency 88 Hz (and its harmonics) which corresponded to the BPF of the aircraft in question. The operating frequency of a mining vehicle cabin, however, is time variant. Therefore any analysis of a mining vehicle cabin should take a range of frequencies into account.

The primary focus of the work described here was to develop an accurate FE model of a mining vehicle cabin that could be used for designing an optimum ANC system and investigating the possibilities for both global and local noise reductions. An attempt has been made to model the cabin so that the sound level response with and without active control can be accurately predicted over a frequency range up to 300 Hz. Using a novel representation of modal damping, accurate FE models of the cabin and its enclosure are developed using ANSYS and then the acoustic and structural models are combined using modal coupling analysis to determine the coupled structural and acoustic response of the cabin to excitation by an interior acoustic source. The numerical model is then verified experimentally for some simple cases. Then, the achievable reduction in both local and global cabin interior noise is investigated numerically. The primary source used for

the initial investigation was a loudspeaker located in the rear of the cabin. This is a simplification of how the actual sound in the cabin is generated as, in practice, the engine excites the cabin structure, which in turn radiates sound into the interior. However, for the purposes of investigating the accuracy of FE modelling and the potential effectiveness of local active noise cancellation, the loudspeaker primary source was considered to be adequate.

2. Analytical modelling

The model of the mining vehicle cabin was developed using ANSYS with the final model comprising 3484 elements and 2856 nodes. The cabin is illustrated in Fig. 1 and the FE model is illustrated in Fig. 2. The first 100 acoustic and 500 structural modes were calculated using the block Lanczos solver and coupled, to obtain the response to a given excitation, using modal coupling theory [12,18,22,23] implemented in MATLAB. As the resonance frequencies of these modes spanned the frequency range up to 600 Hz, it was considered that the response in the frequency range up to 300 Hz was not significantly influenced by modes not considered.

2.1. Summary of modal coupling analysis

Fahy showed that the coupled modal equations of motion for the structure and the cavity are:

$$\ddot{w}_i + \omega_i^2 w_i = -\frac{\rho_0 S}{M_i} \sum_{l=1}^{\infty} \dot{\Phi}_l B_{l,i} + \frac{F_i}{M_i}, \tag{1}$$
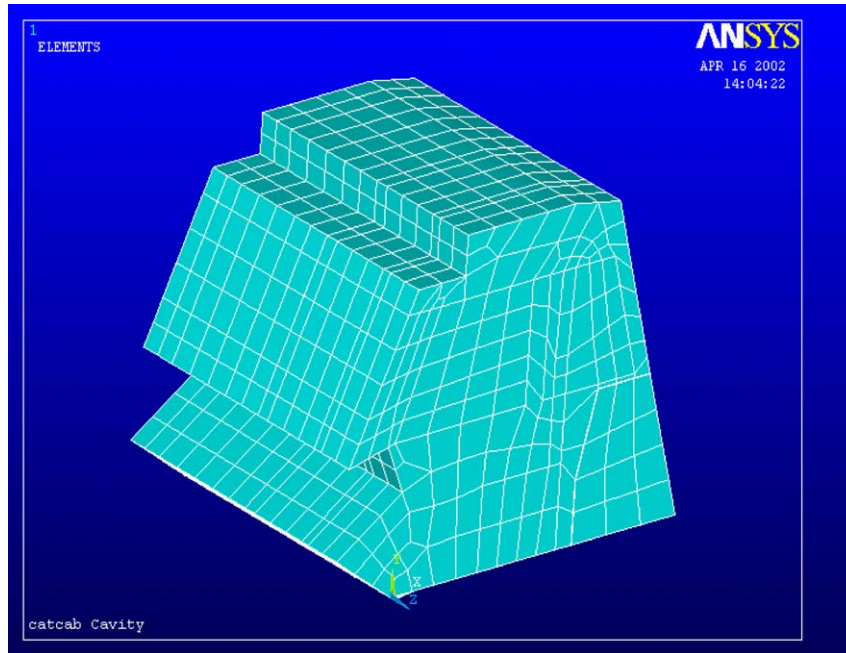

Fig. 1. Photo of Caterpillar mining vehicle cabin.

Fig. 2. Mining vehicle cabin FE model.

$$\ddot{\Phi}_l + \omega_l^2 \Phi_l = \frac{c_0^2 S}{\Lambda_l} \sum_{i=1}^{\infty} \dot{w}_i B_{l,i} - \frac{c_0^2 Q_l}{\Lambda_l}, \tag{2}$$

where w_i is the modal displacement, ω_i is the modal resonance frequency, F_i is the generalized force, and M_i is the modal mass of the ith structural mode. Φ_l is the velocity potential, Q_l the generalized volume velocity, ω_l is the resonance frequency and Λ_l the modal mass of the lth acoustic mode. S is the total surface area of the structure, and $B_{l,i}$ is the non-dimensional coupling coefficient between the lth acoustic mode and ith structural mode:

$$B_{l,i} = \frac{1}{S} \int_s \phi_l(\mathbf{r})\psi_i(\mathbf{r}) \, \mathrm{d}A(\mathbf{r}), \tag{3}$$

where ϕ_l and ψ_i are the respective mode shape functions of the uncoupled acoustic and structural modes. Upon rearranging and solving Eqs. (1) and (2) for arbitrary frequency ω, the equation for pressure in the cavity arising from both structural and acoustic sources written in terms of the acoustic wavenumber with the inclusion of a damping term, $\mathrm{j}\eta_{a_l}\omega_l\omega$, for the cavity is

$$p_l = \frac{\mathrm{j}\rho_0\omega}{\Lambda_l(k_l^2 + \mathrm{j}\eta_{a_l}k_lk - k^2)} \left[-S \sum_{i=1}^{n_s} v_i B_{l,i} + Q_l \right] \tag{4}$$

and the equation for velocity of the structure arising from both structural and acoustic sources with the inclusion of a damping term, $j\eta_{s_i}\omega_i^2$, for the structure is

$$v_i = \frac{j\omega}{M_i(\omega_i^2 + j\eta_{s_i}\omega_i^2 - \omega^2)}\left[S\sum_{l=1}^{n_a} p_l B_{l,i} + F_i\right]. \tag{5}$$

Finally, to arrive at the coupled acoustic response of the system to acoustic sources only, the force term in Eq (5) is set to zero and v_i is substituted into Eq. (4) to yield the resultant pressure of the lth acoustic mode:

$$p_r = \frac{j\rho_0\omega}{\Lambda_l(k_l^2 + j\eta_{a_l}k_lk - k^2)}\left[-S\sum_{i=1}^{n_s}\frac{j\omega}{M_i(\omega_i^2 + j\eta_{s_i}\omega_i^2 - \omega^2)}\left[S\sum_{l=1}^{n_a} p_l B_{l,i}\right]B_{l,i} + Q_l\right], \tag{6}$$

which simplifies to

$$\frac{-j\Lambda_l(k_l^2 + j\eta_{a_l}k_lk - k^2)}{\rho_0\omega}p_r = j\omega S^2\sum_{i=1}^{n_s}\sum_{l=1}^{n_a}\frac{B_{l,i}B_{l,i}}{M_iZ_i}p_l + Q_l. \tag{7}$$

Summarized in matrix form, the coupled acoustic response of a system (resultant pressure) in which acoustic sources but no structural forces act, is

$$\boldsymbol{p} = \boldsymbol{Z}_q^{-1}\boldsymbol{Q}, \tag{8}$$

where $\boldsymbol{p}$ is a $(n_a \times 1)$ vector, the elements of which represent the pressure amplitude of each acoustic mode, $\boldsymbol{Q}$ is an $(n_a \times 1)$ vector, the elements of which represent the relative contribution of the acoustic volume velocity sources to each acoustic mode, and $\boldsymbol{Z}_q$ is the $(n_a \times n_a)$ acoustic modal input impedance matrix, the elements of which are

$$Z_q(u,u) = j\omega S^2\sum_{i=1}^{n_s}\frac{B_{u,i}B_{u,i}}{M_iZ_i} - \frac{j\Lambda_u(k_u^2 + j\eta_{a_u}k_uk - k^2)}{\rho_0\omega} \quad \text{(diagonal terms)}, \tag{9}$$

$$Z_q(u,v) = j\omega S^2\sum_{i=1}^{n_s}\frac{B_{u,i}B_{v,i}}{M_iZ_i} \quad \text{(off-diagonal terms)}, \tag{10}$$

where the indices u and v are the uth and vth acoustic modes from 1 to n_a.

Of important note here is the way in which values for structural and acoustic damping were defined. In previous work, Cazzolato [18] arbitrarily specified a constant 2% damping across all structural and acoustic resonant frequencies for his curved panel with backing cavity model. However, here measured transfer functions between a loudspeaker sound source (P1–P5) (ratio of the acoustic pressure to the source volume velocity) and a microphone in the cabin (M1–M8) were used to estimate both acoustic and structural damping in the following way. The response in the cabin was first simulated at a number of locations (P1–P5) assuming a constant 2% damping across all modes. Then the damping for each mode was manually adjusted so that the numerical predictions matched the measured transfer functions as best as possible through a trial and error process.

2.2. Summary of quadratic optimization theory

Quadratic optimization theory (QOT) [24] was used to determine the unique control source signal amplitudes and phases for minimising the cost function at a number of error sensor locations and subsequently to predict the optimal level of control achievable in the cabin.

The cost function to be minimized is

$$J_p = \sum_{i=1}^{e} |p_{t_i}|^2 = \boldsymbol{p}_t^{\mathrm{H}} \boldsymbol{p}_t = (\boldsymbol{p}_p + \boldsymbol{Z}\boldsymbol{q}_s)^{\mathrm{H}}(\boldsymbol{p}_p + \boldsymbol{Z}\boldsymbol{q}_s), \tag{11}$$

where $\boldsymbol{p}_t$ is the vector of total sound pressures at the error sensor locations, made up of the combined primary, $\boldsymbol{p}_p$, and controlled, $\boldsymbol{p}_s$, pressure fields at the same locations. The vector, $\boldsymbol{q}_s$, represents the control source volume velocities and the transfer impedance matrix, $\boldsymbol{Z}$, is defined as

$$\boldsymbol{Z} = \begin{bmatrix} z_{11} & z_{12} & \cdots & z_{1c} \\ z_{21} & z_{22} & \cdots & z_{2c} \\ \vdots & \vdots & \vdots & \vdots \\ z_{e1} & z_{e2} & \cdots & z_{ec} \end{bmatrix}, \tag{12}$$

where the elements of $\boldsymbol{Z}$ are found by measuring the transfer function between each error sensor and each control source input signal in turn, with the primary source turned off, such that

$$\boldsymbol{p}_s = \boldsymbol{Z}\boldsymbol{q}_s. \tag{13}$$

Expanded and represented in quadratic form, the cost function becomes:

$$J_p = \boldsymbol{q}_s^{\mathrm{H}} \boldsymbol{A} \boldsymbol{q}_s + \boldsymbol{q}_s^{\mathrm{H}} \boldsymbol{b} + \boldsymbol{b}^{\mathrm{H}} \boldsymbol{q}_s + \boldsymbol{c}, \tag{14}$$

where $\boldsymbol{A}$, $\boldsymbol{b}$, and $\boldsymbol{c}$ are the coefficients of a quadratic equation, given by

$$\boldsymbol{A} = \boldsymbol{Z}^{\mathrm{H}} \boldsymbol{Z}, \tag{15}$$

$$\boldsymbol{b} = \boldsymbol{Z}^{\mathrm{H}} \boldsymbol{p}_p, \tag{16}$$

$$\boldsymbol{c} = \boldsymbol{p}_p^{\mathrm{H}} \boldsymbol{p}_p. \tag{17}$$

The optimal set of secondary control source strengths that will minimize J_p is

$$\boldsymbol{q}_{s(opt)} = -\boldsymbol{A}^{-1} \boldsymbol{b}. \tag{18}$$

As the matrix, A, is not square, it is necessary to use the pseudo inverse, $\boldsymbol{A}^{-1} = (\boldsymbol{A}^{\mathrm{H}} \boldsymbol{A})^{-1} \boldsymbol{A}^{\mathrm{H}}$.

Note that if the same number of error sensors as control sources is used, quadratic optimization will predict that zero sound pressure can be achieved at all error sensors. So in practice, either a limit is set on the controller accuracy or more error sensors than control sources are used.

3. Experimental work

3.1. Primary source volume velocity measurement

The use of modal coupling theory assumes that both the primary and control acoustic sources are monopole constant volume velocity sources. Therefore, for verification with the FE model, it was necessary to measure the volume velocity output of the acoustic source, in this case a loudspeaker backed by a small enclosure. Anthony and Elliott [25] outline three techniques for volume velocity measurement. They compare two methods with laser velocimetry; namely, measurement of the internal source pressure, and using a moving-coil loudspeaker as an output transducer (known as Salava's method). They concluded that Salava's method is superior in terms of measurement accuracy and harmonic distortion. However, all three of these methods are difficult to execute experimentally. Snyder and Hansen [26] describe a fourth method for measuring volume velocity. Using this method, the internal pressure generated by a loudspeaker in a sealed backing enclosure is measured and converted into volume velocity by using the calculated impedance of the volume. This method is easier to implement experimentally, and was the one chosen for the work described here.

3.2. Experimental work using the mining vehicle cabin

Experimental work was carried out inside a Caterpillar mobile mining vehicle cabin to gain further understanding of its acoustic properties, and more importantly, to verify the model. Externally, the cabin was 2.4 m long, 1.5 m wide, and 1.7 m tall. The source and microphone positions referred to in the text to follow are identified in Fig. 3.

Testing on the cabin was divided into two stages. In the first stage, the objective was to measure transfer functions that could be used to confirm the accuracy of the FE and modal coupling models in predicting the interior sound pressure field generated by a constant volume source, which was approximated using a small loudspeaker backed by a small enclosure. This required the measurement of transfer functions between a microphone in the cabin and a microphone inside the primary source speaker enclosure, and then converting the result to a ratio of cabin pressure to source volume velocity [26] to make the measurements compatible with the ANSYS/MATLAB simulations. A PULSE system signal generator (B&K multi-channel data acquisition unit type 2816 with generator module type 3107) amplified via a Playmaster Pro Series 3 power amplifier was used to drive an Excel Seas 110 mm diameter speaker with random noise up to 400 Hz. B&K type 4133 microphones connected to a B&K type 2804 preamplifier were used to measure the required transfer functions, with one microphone being securely placed inside the speaker housing, and the other strategically located in the cabin.

Various randomly selected positions of sensors and sound sources were used to verify the FE model using a constant volume velocity loudspeaker source. Eight cabin microphone positions and five primary source positions were tested. The results of the model verification procedure are presented in Section 4.1.

For the second stage of testing, the objective was to measure transfer functions that could be used to predict the level of local control and the extent of global control achievable in the cabin for various error sensor and control source configurations when squared pressure is minimized.
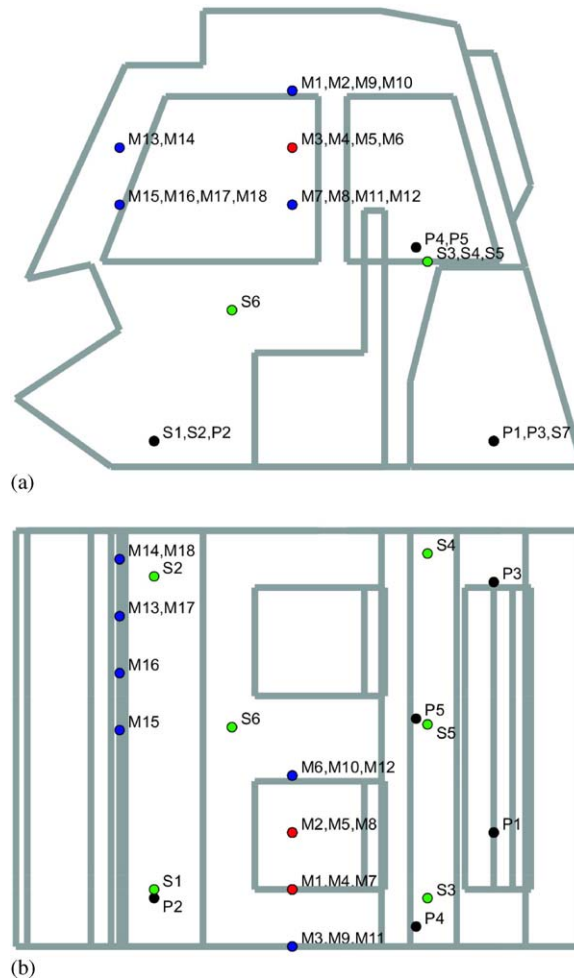
Fig. 3. Side (a) and front (b) view of the interior of the mining vehicle cabin showing the microphone (M) primary source (P) and control source (S) locations referred to in the following text and figures.

Transfer functions between the acoustic pressure at 18 different cabin microphone locations and the source volume velocity for six different source locations were measured. The source volume velocity was determined using a microphone in the backing cavity of the loudspeaker enclosure as described by Snyder and Hansen [26]. QOT [24] was applied to these transfer functions to ascertain the optimum level of control achievable inside the cabin ("off-line" control).

Real time controllers are usually limited by how many channels they can control simultaneously. The EZANC II system used for the work described here has a maximum of ten input and ten output channels allowing up to nine control sources to be used to control a maximum of nine error sensors. For realistic results to be determined using QOT, the number of error sensors should exceed the number of control sources. If the number of error sensors is equal to the number of control sources, it is theoretically possible to achieve zero sound pressure at each error sensor. If there are more control sources than error sensors, the system is over determined

and there is no unique solution for optimal control source strengths. For these reasons, eight error sensors and six control sources were used for "realistic" control predictions. The eight microphone locations nearest the volume that surrounds the driver's head if he/she were sitting in the cabin were selected for this purpose. Transfer functions were measured from the control source volume velocity to other non-error microphone locations to ascertain the effect that controlling noise level at one location had on other locations in the cabin. Transfer functions at four microphone locations, each within $\lambda/6$ (at 300 Hz) of one of the eight error sensors were measured, as well as six more "non-error" microphone locations well away from the error microphones (minimum separation $\lambda/2$ at 300 Hz), where λ is the wavelength of sound. All of these transfer functions were duplicated in the FE model and correlated with the experimental data. The results are presented in Section 4.2.

The six different control source locations and primary source location used for the off-line control analysis were chosen based on their practicality and potential impact on the interior sound field. That is, the locations were chosen to be as close as possible to enclosure corners where the sources are likely to be able to drive all acoustic modes excited in the enclosure.

Since accurately measuring the acoustic PE of a large cavity requires a multitude of sensors, acoustic PE reduction predictions were performed solely using the FE model. A range of primary disturbance locations were also selected for the acoustic PE reduction predictions of the FE model. This was because it was found that the location of the primary source had a significant impact on the controlled response. Hence every combination of control sources was used several times in simulations to control a primary source at each specific location. The acoustic PE reduction predictions are discussed in Section 4.3.

4. Discussion of results

4.1. Verification of the finite element model

The results of the correlation between calculated and experimental frequency responses in the cabin are presented in two forms. For each control source and sensor combination shown, the response at the sensor location is presented first as a one-third octave band average, and then as a spectrum up to 300 Hz. To calculate the band averaged amplitude level, the time averaged values of the pressure squared at each frequency in a one-third octave band were averaged and then converted to decibels.

For the simulated response curves up to 300 Hz, spatial averaging was used. The response was averaged over the closest 50 nodes to the sensor co-ordinates selected; this represented an effective volume of the approximate size of a 10 cm cube. This had the effect of averaging out any problems caused by slight modelling inaccuracies and could be justified in a similar way that 1/3 octave band data are used for frequency averaging purposes. Modelling inaccuracies are a result of assumptions and approximations made regarding the dimensions of the cabin, its material properties, connections, seals, boundary conditions, and damping.

Measured and predicted transfer functions between several control source locations and one microphone location are shown in Fig. 4. These locations are different to those used to optimize the modal damping values for the numerical model. Considering the complex nature of the
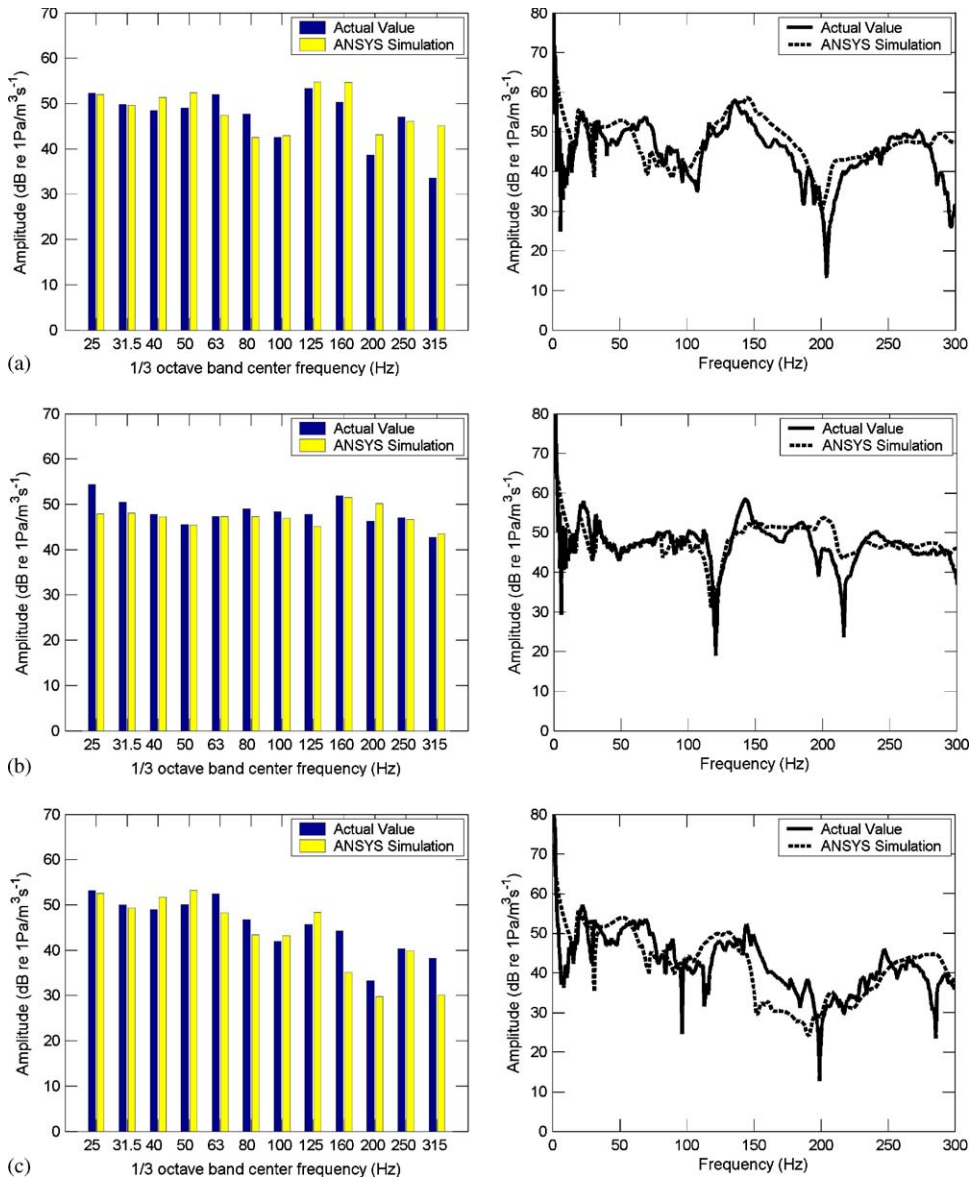
Fig. 4. Correlation between predicted and measured transfer functions. One-third octave results are shown on the left and narrow band results on the right. Transfer functions are the ratio of the acoustic pressure at the microphone location to the volume velocity of the loudspeaker source. (a) Source position P1, microphone position M2. (b) Source position P2, microphone position M5. (c) Source position P3, microphone position M3.

environment modelled, the correlation between the measured transfer functions and simulated responses is considered acceptable for ANC predictions. The model predicts the basic shape of the measured transfer function, and the amplitude prediction is reasonable. The model is also robust to alternative combinations of control source and sensor locations, with the model predicting the

changes that different combinations cause. Errors were only significant at anti-resonant frequencies where the coherence between the two signals used to derive the transfer function was poor.

The model and measurements concur that the acoustic cavity modes dominate the overall system response. Many of the smaller ''bumps'' observed in the measured transfer functions are due to the presence of the weaker structural modes. However, these had minimal impact on the overall shape of the transfer function curve, and are not evident in the simulated model results. However, it is important to include the structural response in the model as that will allow future investigation of active control when the unwanted sound results from vibration of the cabin walls.

Presentation of the data in band averaged form shows that the model is reasonably consistent with the real structure. In the majority of frequency bands, an amplitude error of less than 5 dB was achieved. In bands where there was a greater difference it was usually due to the simulated level being much lower than the measured response over that frequency band (particularly in the 25 and 31.5 Hz bands). The coherence between the two signals making up the transfer function measurement at frequencies in these bands was poor, so as for the narrow band comparisons, poor agreement between measured and predicted results can be expected for these bands.

4.2. Off-line control

Figs. 5(a)–(c) show the measured and predicted primary sound field at a microphone, and the off-line control prediction using QOT with six control sources for both measured and simulated transfer functions. The controlled sound field prediction curves using the cabin measurements have been passed through a function that averaged the original curve over 2 Hz bands and then fitted the resultant points with a polynomial of degree 50. This was done because the original predicted controlled sound fields calculated using QOT were highly scattered in nature. This effect is most likely to be a result of poor conditioning in the matrices involved in the QOT derivation of optimal control source strengths. Alternating the order of error sensors in the Z matrix was attempted to eliminate the problem, but with no success.

Broadband reduction up to 30 dB is predicted using off-line control at the error microphones and there is even some reduction at the microphones close to those being controlled. However, little or no reduction is seen at the microphones furthest away from the error microphones. Only the results of a single microphone from each of the three location types are shown here. As with the results in Section 4.1, reasonable agreement was achieved between the measured and simulated transfer functions in Figs. 5(a)–(c). Over the 300 Hz frequency range of interest, the FE model broadly estimates the amplitude of the primary field transfer function in the mining vehicle cabin, and then predicts with good accuracy the level of reduction that occurs at each of the 18 microphone locations measured when the eight error microphones near the driver's head are controlled with six control sources.

With polynomial fitting, the controlled sound field transfer function derived from cabin measurements is similar to that of the optimized FE model transfer function. Furthermore, the trend over the three general categories of microphone locations tested (error sensors, non-error sensors near the error sensors, and non-error sensors well away from the error sensors) is the same for the two sets of data. Both data sets show large reductions at the error sensors, moderate reduction at the non-error sensors nearby, and little reduction or even an increase in noise level at
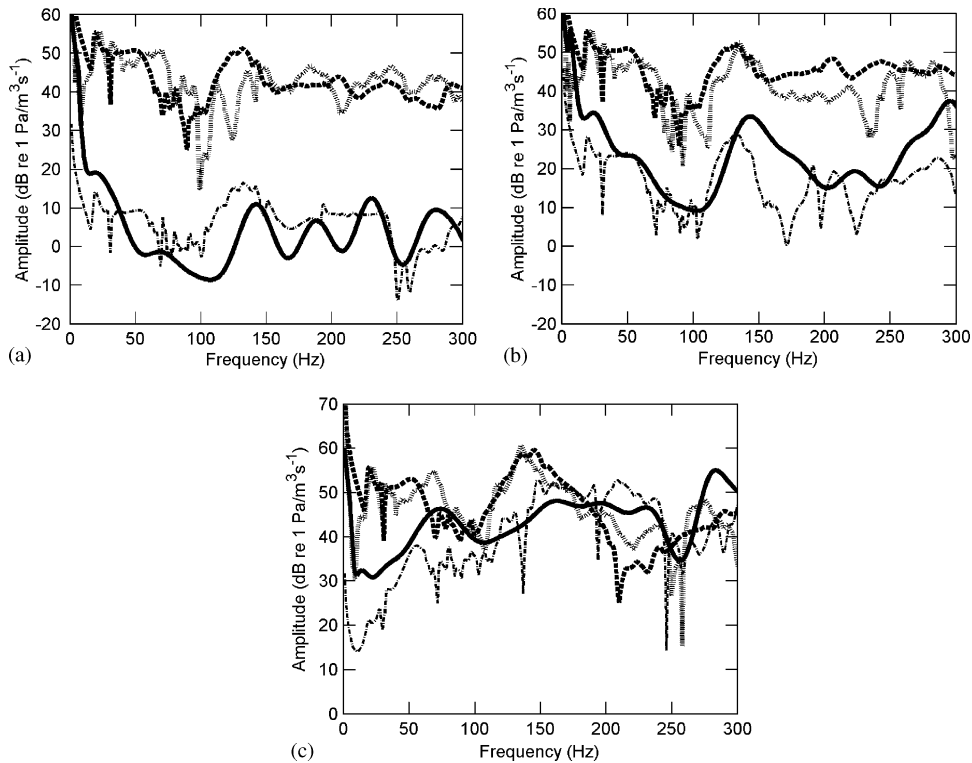
Fig. 5. Optimal local control prediction and correlation between predicted and measured transfer functions using six sources and eight error sensors. Transfer functions represent the ratio of the acoustic pressure at a microphone in the cabin and the volume velocity of the primary loudspeaker source (P1). *Dotted line*: Measured primary sound field in cabin. *Dashed line*: Simulated primary sound field using FE model. *Solid line*: Controlled sound field prediction using cabin measurements. *Dash–dot line*: Controlled sound field prediction using FE model. (a) Error microphone M5. (b) Microphone M9, within $\lambda/6$ (at 300 Hz) of an error sensor (M5). (c) Microphone M13, microphone $5\lambda/7$ (at 300 Hz) away from the closest error sensor (M6).

the non-error sensors well away from the error sensors. This agrees with the results obtained by Elliott et al. [7]. It also highlights the potential for local control and the impracticality of global control in the mining vehicle cabin using loudspeaker control sources.

There is evidence suggested by Cazzolato [18], and also by Kestell et al. [27] that the areas of local control can be expanded into larger zones by using energy density sensing. An energy density sensor suggested by Cazzolato [18], comprises four microphones, three of which are located along the three orthogonal cartesian axes and the fourth in an arbitrary plane. In theory, if an energy density sensor can be used in place of a microphone and arranged in a control system such that the acoustic pressures at the four microphones of the energy density sensor are all driven to zero (this could be achieved with four control sources), then it would be possible to create a zone of quiet large enough to enclose the head of the driver up to frequencies around 300 Hz, since energy density strategies are expected to produce large ellipsoid shaped zones of quiet (with the larger radius equal to $\lambda/4$) around the error sensor (Elliott and Garcia-Bonito [28]). The EZANC II

controller could then be fully utilized with a second energy density probe for the passenger and four more control sources. This concept is the subject of ongoing work.

4.3. Prediction of the effect of active noise control using the model

Having established that the FE model is a sufficient representation of its real counterpart, the model was used to run simulations to predict the reduction of total acoustic PE achievable in the mining vehicle cabin. In a simulation environment, physical parameters such as location and number of control sensors and control sources can be modified easily, saving experimental time. Trends can also be obtained much faster, as the effects of changes in the physical parameters on the frequency responses can be seen immediately. Working in a simulation environment has the additional advantage of allowing one to trial ideas that at the time are not practically feasible, to determine if they are worthy of expending the effort on implementation at a later date (for example, the use of 32 error sensors and 16 control sources in a mining vehicle cabin control system, as will be detailed shortly).

The simulations used the locations of the primary and control sources specified in Section 3 to calculate the response at each of the 2856 nodes in the model before and after secondary sources were introduced. The average of the squared pressures at all of these nodes was used as a good approximation to the acoustic PE in the cabin and the quantity minimized was the sum of the calculated squared pressures at the 2856 nodal locations. Originally it was intended to optimize the number and location of the control sources by using a genetic search algorithm. However, the estimated length of time to do such a search and the computer power required to do it rendered the approach impractical. Hence the control sources were located in the corners of the cabin, where they were best able to excite most of the cabin modes.

For each primary source position, the optimally controlled response using one to eight control sources and the 2856 error sensors (one for each node in the model) was calculated. In Fig. 6 the response when using one control source and all eight control sources is shown for each of the three primary source positions. The use of any number of control sources between one and eight resulted in a performance that was within the two extremes shown.

The results in Fig. 6 coincide with the conclusions of Zander [14]. Inspection of these results reveals that the effect of the location of the control source with respect to the primary source is more important than the number of control sources in terms of achievable reduction in the acoustic PE. However it can be seen that in all cases, eight control sources provide greater reduction in acoustic PE than one source and this is more noticeable at higher frequencies.

The lack of control at higher frequencies is a result of the high modal overlap, which is controlled by the modal density and the modal damping, both of which are high. The acoustic and structural modal damping, modal density, and modal overlap are shown as a function of frequency in Tables 1 and 2.

The difference in control performance for the three primary source locations considered is due to the relative locations of the primary source and control sources. Considering the highest frequency in the frequency range of interest (300 Hz), for the results shown in Figs. 6(a) and (b), the primary source is never closer than $3\lambda/5$ to any control source. For the results shown in Figs. 6(c) and (d), the primary source is within $7\lambda/10$ of a control source, and for the results shown in Figs. 6(e) and (f), the primary source is within $3\lambda/100$ of one of the control
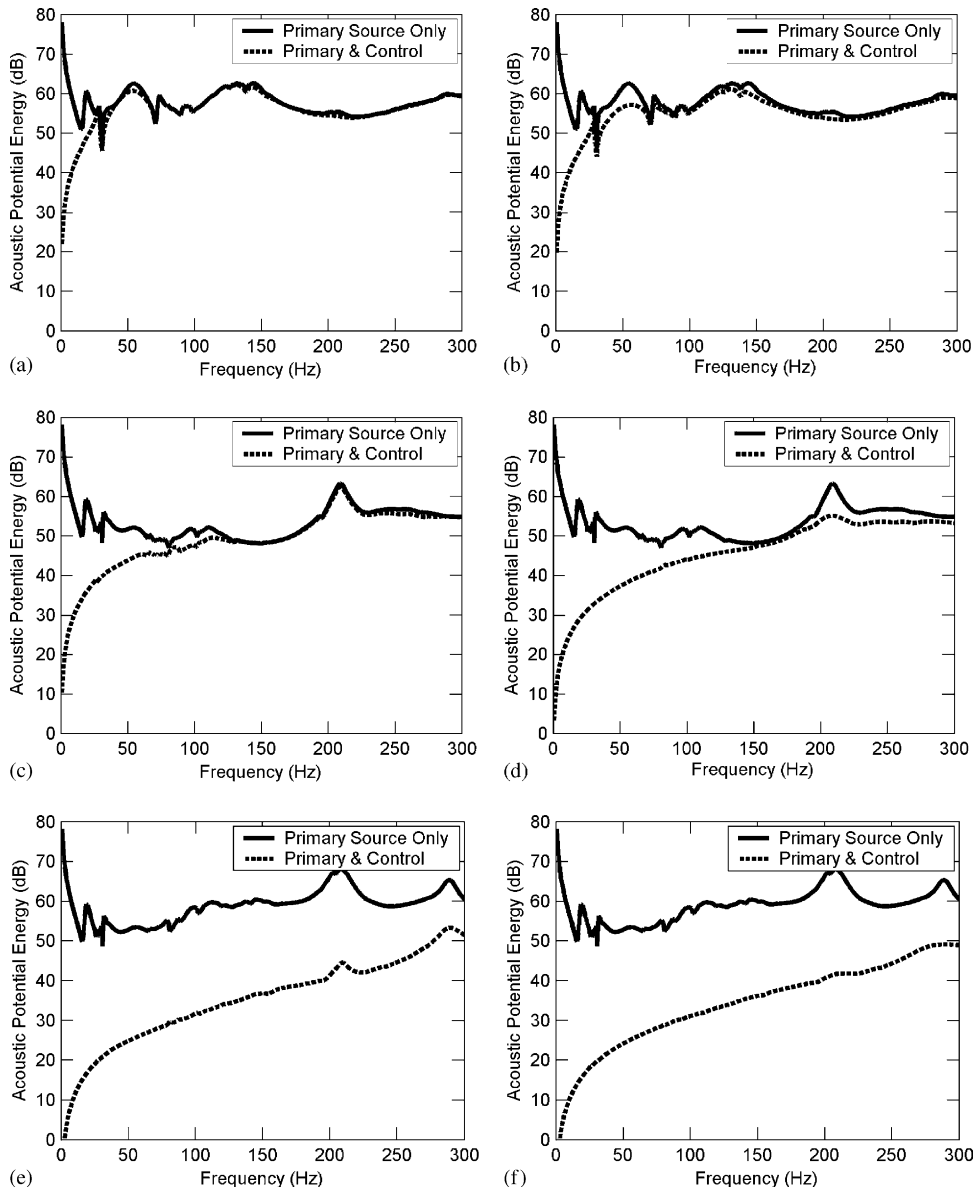
Fig. 6. Predicted primary and controlled acoustic PE levels in the mining vehicle cabin. (a) Primary source location P1, control source location S1. (b) Primary source location P1, all eight control sources. (c) Primary source location P2, control source S1. (d) Primary source location P2, all eight control sources. (e) Primary source location P3, control source S1. (f) Primary source location S3, all eight control sources.

sources. This agrees with the results obtained by Nelson et al. [1] for an acoustical environment of high modal density.

In Fig. 7, possible reductions in acoustic PE using 1, 8 or 16 control sources and 8, 16, 32 and 2856 error sensors are shown for one primary source location that is relatively far (0.6λ at 30 Hz

Table 1
Acoustic modal properties of the mining vehicle cabin model

| 1/3 Octave band centre frequency (Hz)	Modal density of band	Average modal loss factor of modes in band	Band modal overlap (cavity)
25	0.00	0.00	0.00
31.5	0.00	0.00	0.00
40	0.00	0.00	0.00
50	0.07	0.35	1.25
63	0.00	0.00	0.00
80	0.00	0.00	0.00
100	0.04	0.30	1.15
125	0.07	0.26	2.26
160	0.08	0.23	3.09
200	0.08	0.11	1.70
250	0.17	0.15	6.26
315	0.15	0.25	12.0
400	0.26	0.23	24.3

Table 2
Structural modal properties of the mining vehicle cabin model

1/3 Octave band centre frequency (Hz)	Modal density of band	Average modal loss factor of modes in band	Band modal overlap (structure)
25	0.29	0.02	0.14
31.5	0.50	0.07	1.02
40	0.70	0.20	5.60
50	0.50	0.20	5.00
63	0.60	0.08	3.02
80	0.94	0.02	1.51
100	0.88	0.02	1.77
125	0.86	0.02	2.16
160	1.00	0.10	15.2
200	1.10	0.05	10.9
250	1.15	0.02	5.76
315	1.25	0.02	7.90
400	1.34	0.02	10.7

and 6λ at 300 Hz) from any of the control sources. The cost function was the sum of the squared sound pressures at the error sensors and the control sources were located in the corners of the cabin, where they were best able to excite most of the cabin modes.

It can be seen from Fig. 7 that as the number of error sensors are reduced, there is more of an increase in the overall cabin acoustic PE at higher frequencies, even though the sum of the squared pressures is minimized. Restricting the error sensors to a small volume results in more effective
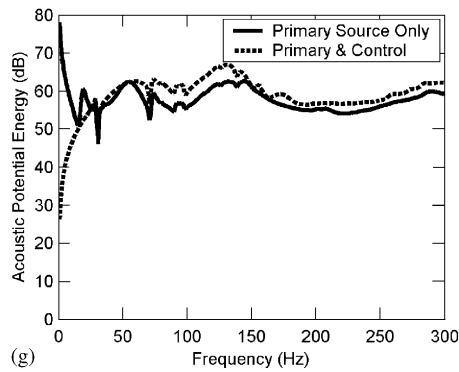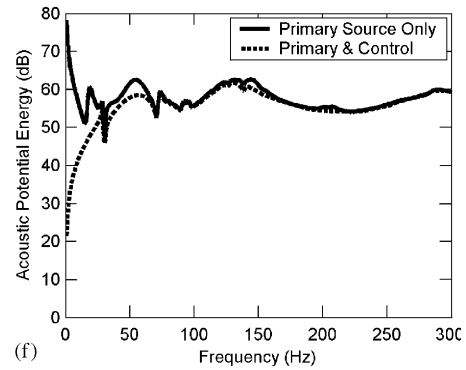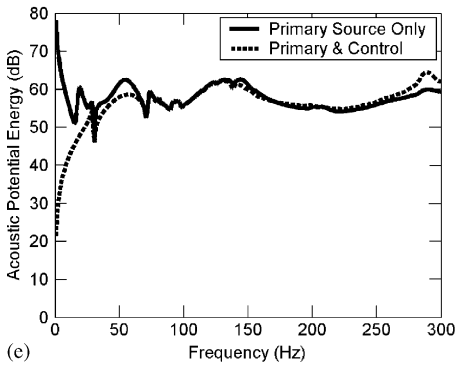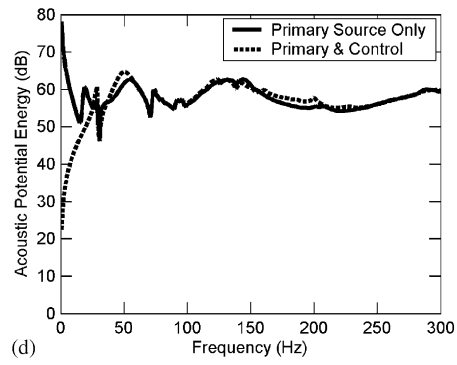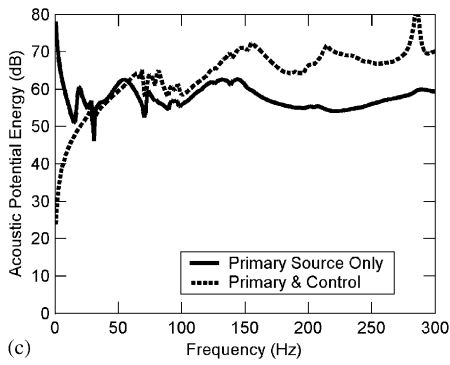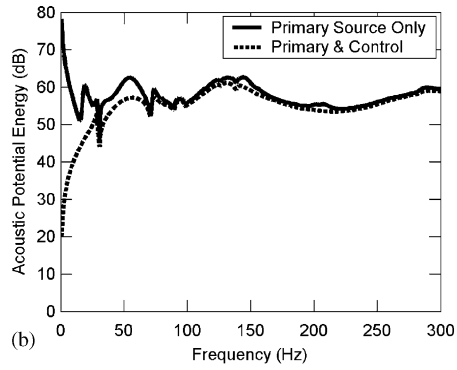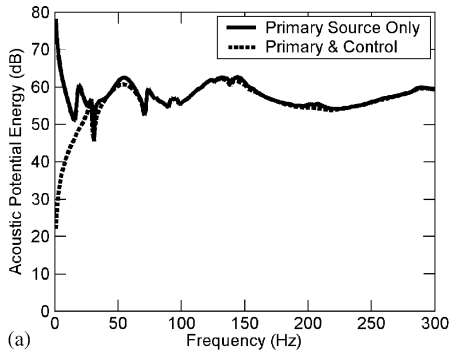
global control (Fig. 7(d)), than achieved with the same number uniformly distributed. It is also seen that increasing the number of control sources above a minimum number can also have an adverse effect on the acoustic PE at higher frequencies.

5. Conclusions

By introducing individual modal damping values and matching them with many different transfer function measurements, an accurate FE model of a mining vehicle cabin has been developed. The model has been shown to accurately predict both structural and acoustic resonance frequencies and mode shapes. The FE model was used with modal coupling analysis to accurately predict frequency response functions between acoustic source volume velocities and sound pressures at microphones in the cabin over a frequency range up to 300 Hz.

The measured transfer functions used for verifying the numerical model were also used in off-line control experiments. Quadratic optimization theory was applied to the measurements and FE model simulations to predict the optimal control achievable using six control sources and eight error microphones. Good agreement was again obtained, with the two sets of results indicating that a significant noise reduction at the error sensors was possible but global control was not feasible for control sources placed a relatively large distance ($> \lambda/2$) from the primary source. This confirmed the initial assumption that global control is difficult to achieve in a complex three-dimensional enclosure by using small acoustic sources to minimize the squared sound pressure, as suggested by Elliott et al. [7] for enclosures of high modal density.

Numerical simulations that predicted the reduction of acoustic PE across the cavity were also performed. The FE model and accompanying MATLAB code used for post-processing assumed a primary volume velocity source. As expected from previous work by Nelson et al. [1], it was found that the acoustic PE inside the cabin can be significantly reduced if a control source is placed in close proximity to the primary source. This is viable for experimental purposes, but may not be applicable to a real vehicle where the primary noise originates from the engine and is radiated into the cabin by vibration of the walls. However, for this more practical case, it may be possible to use distributed acoustic sources that cover the entire interior solid walls, roof and floor of the cabin to provide an effective cancelling sound field [29]. This is the subject of future work.

Increasing the number of sensors and/or increasing the number of control sources located remotely from the primary source had little impact on the overall acoustic PE in the cabin because the modal overlap was too high. Control at lower frequencies was marginally improved with the use of more control sources, which was previously demonstrated by Zander [14], but the tendency for the energy level to increase rather than decrease at other frequencies was also observed. This supported the results obtained previously in off-line experiments using quadratic optimization theory.

Fig. 7. Predicted primary and controlled acoustic PE levels in the mining vehicle cabin with the primary source relatively far from any control source. (a) 1 control source, 2856 error sensors. (b) 8 control sources, 2856 error sensors. (c) 8 control sources, 8 error sensors uniformly distributed. (d) 8 control sources, 8 error sensors in a spherical volume of radius 0.3 m. (e) 8 control sources, 16 error sensors uniformly distributed. (f) 8 control sources, 32 error sensors uniformly distributed. (g) 16 control sources, 32 error sensors uniformly distributed.

Areas of local control can be expanded into larger zones using an energy density sensing strategy and this is the subject of ongoing work.

Acknowledgements

References

[1] P.A. Nelson, A.R.D. Curtis, S.J. Elliott, A.J. Bullmore, The active minimization of harmonic enclosed sound fields, Part I: theory, *Journal of Sound and Vibration* 117 (1) (1987) 1–13.

[2] A.J. Bullmore, P.A. Nelson, A.R.D. Curtis, S.J. Elliott, The active minimization of harmonic enclosed sound fields, Part II: computer simulation, *Journal of Sound and Vibration* 117 (1) (1987) 15–33.

[3] S.J. Elliott, A.R.D. Curtis, A.J. Bullmore, P.A. Nelson, The active minimization of harmonic enclosed sound fields, Part III: experimental verification, *Journal of Sound and Vibration* 117 (1) (1987) 35–58.

[4] A.J. Bullmore, P.A. Nelson, S.J. Elliott, Theoretical studies of the active control of propeller-induced cabin noise, *Journal of Sound and Vibration* 140 (2) (1990) 191–217.

[5] S.J. Elliott, P.A. Nelson, I.M. Stothers, C.C. Boucher, Preliminary results of in-flight experiments on the active control of propeller-induced cabin noise, *Journal of Sound and Vibration* 128 (2) (1989) 355–357.

[6] S.J. Elliott, P.A. Nelson, I.M. Stothers, C.C. Boucher, In-flight experiments on the active control of propeller-induced cabin noise, *Journal of Sound and Vibration* 140 (2) (1990) 219–238.

[7] S.J. Elliott, P. Joseph, A.J. Bullmore, P.A. Nelson, Active cancellation at a point in a pure tone diffuse sound field, *Journal of Sound and Vibration* 120 (1) (1988) 183–189.

[8] C.M. Dorling, G.P. Eatwell, S.M. Hutchins, C.F. Ross, S.G.C. Sutcliffe, A demonstration of active noise reduction in an aircraft cabin, *Journal of Sound and Vibration* 128 (2) (1989) 358–360.

[9] S. Johansson, P. Persson, I. Claesson, Active control of propeller-induced noise in an aircraft mock-up, *Proceedings of Active 99*, 1999, pp. 741–752.

[10] D.R. Thomas, P.A. Nelson, S.J. Elliott, Active control of the transmission of sound through a thin cylindrical shell, Part I: the minimization of vibrational energy, *Journal of Sound and Vibration* 167 (1) (1993) 91–111.

[11] D.R. Thomas, P.A. Nelson, S.J. Elliott, Active control of the transmission of sound through a thin cylindrical shell, Part II: the minimization of acoustic potential energy, *Journal of Sound and Vibration* 167 (1) (1993) 113–128.

[12] S.D. Snyder, C.H. Hansen, The design of systems to actively control periodic sound transmission into enclosed spaces, Part I: analytical models, *Journal of Sound and Vibration* 170 (4) (1994) 433–449.

[13] S.D. Snyder, C.H. Hansen, The design of systems to actively control periodic sound transmission into enclosed spaces, Part II: mechanisms and trends, *Journal of Sound and Vibration* 170 (4) (1994) 451–472.

[14] A.C. Zander, Influence of Error Sensor and Control Source Configuration and Type upon the Performance of Active Noise Control Systems, PhD Dissertation, The University of Adelaide, Adelaide, Australia, 1994.

[15] M. Alvelid, Optimisation of secondary sources for active noise control in a FE-model of an aircraft cabin, *Proceedings of Inter Noise 93*, 1993, pp. 65–70.

[16] E. Carletti, G. Miccoli, I. Vecchi, Earth-moving cab enclosed sound field active control simulation, *Proceedings of Inter Noise 96*, 1996, pp. 1183–1186.

[17] Y. Dai, C. Fuller, Numerical simulation of active control of interior noise in a business jet with point force actuators—optimization of transducers, *Proceedings of Inter Noise 95*, 1995, pp. 533–536.

[18] B.S. Cazzolato, Sensing Systems for Active Control of Sound Transmission into Cavities, PhD Dissertation, The University of Adelaide, Adelaide, Australia, 1999.

[19] B.S. Cazzolato, C.H. Hansen, Active control of sound transmission using structural error sensing, *Journal of the Acoustical Society of America* 104 (5) (1998) 2878–2889.

[20] J.F. Unruh, S.A. Dobosz, Fuselage structural-acoustic modeling for structure-borne interior noise transmission, *Journal of Vibration, Acoustics, Stress, and Reliability in Design* 110 (1988) 226–233.

[21] S.H. Sung, D.J. Nefske, A coupled structural-acoustic finite element model for vehicle interior noise analysis, *Journal of Vibration, Acoustics, Stress, and Reliability in Design* 106 (1984) 314–318.

[22] L. Pope, On the transmission of sound through finite closed shells: statistical energy analysis, modal coupling, and non-resonant transmission, *Journal of the Acoustical Society of America* 50 (3) (1971) 1004–1018.

[23] F. Fahy, *Sound and Structural Vibration: Radiation, Transmission, and Response*, Academic Press, London, 1985.

[24] C.H. Hansen, *Understanding Active Noise Cancellation*, Spon Press, London, 2001.

[25] D.K. Anthony, S.J. Elliott, A comparison of three methods of measuring the volume velocity of an acoustic source, *Journal of the Audio Engineering Society* 39 (5) (1991) 355–366.

[26] S. Snyder, C. Hansen, Active noise control in ducts; Some physical insights, *Journal of the Acoustical Society of America* 86 (1989) 184–194.

[27] C.D. Kestell, B.S. Cazzolato, C.H. Hansen, Active noise control in a free field with virtual sensors, *Journal of the Acoustical Society of America* 109 (1) (2001) 232–243.

[28] S. Elliott, J. Garcia-Bonito, Active cancellation of pressure and pressure gradient in a diffuse sound field, *Journal of Sound and Vibration* 186 (4) (1995) 696–704.

[29] C.R. Fuller, M.E. Johnson, J.R. Griffin, Active–passive control of aircraft interior boundary layer noise using smart foam, AIAA Paper No. 2000-2041, 2000.